(This is a sample cover image for this issue. The actual cover is not yet available at this time.)

Biochimica et Biophysica Acta 1822 (2012) 906–917

Contents lists available at SciVerse ScienceDirect

Biochimica et Biophysica Acta

journal homepage: www.elsevier.com/locate/bbadis

Toxic effects of expanded ataxin-1 involve mechanical instability of the nuclear membrane

Lisa Mapelli [a,1,2], Claudio Canale [b,1], Daniela Pesci [c,1], Stefania Averaimo [a], Fabiana Guizzardi [a,3], Valentina Fortunati [c], Laura Falasca [d], Mauro Piacentini [c,d], Alessandra Gliozzi [e,f], Annalisa Relini [e,f,4], Michele Mazzanti [a,4], Carla Jodice [c,f,4,*]

[a] Department of Biomolecular Science and Biotechnology, University of Milan, Milan, Italy
[b] Facility of Nanobiotechnology, Italian Institute of Technology, Genoa, Italy
[c] Department of Biology, University of Tor Vergata, Rome, Italy
[d] National Institute for Infectious Diseases, IRCCS "L. Spallanzani", Rome, Italy
[e] Department of Physics, University of Genoa, Genoa, Italy
[f] Inter-University Research Centre on the Molecular Basis of Neurodegenerative Diseases (CIMN), Italy

ARTICLE INFO

Article history:
Received 8 August 2011
Received in revised form 26 January 2012
Accepted 30 January 2012
Available online 4 February 2012

Keywords:
Spinocerebellar ataxia type 1
Ataxin 1
Polyglutamine disease
Neurodegeneration
Membrane
Unregulated ionic pathway

ABSTRACT

Ataxin 1 (ATXN1) is the protein involved in spinocerebellar ataxia type 1, one of nine dominantly inherited neurodegenerative diseases triggered by polyglutamine expansion. One of the isolated polyglutamine tracts properties is to interact with lipid bilayers. Here we used a multidisciplinary approach to test whether one of the mechanisms responsible for neuronal degeneration involves the destabilization of the nuclear membrane. We thus analyzed the interaction between ATXN1 and lipid membranes, both on cellular models and on artificial lipid bilayers, comparing pathological expanded polyglutamine and histidine interrupted non-harmful polyglutamine tracts of the same length. The toxicity of the different constructs was tested in transiently transfected COS1 cells. Cells expressing pathological ATXN1 presented a significantly higher frequency of anomalous nuclei with respect to those expressing non-harmful ATXN1. Immunofluorescence and electron microscopy showed severe damage in the nuclear membrane of cells expressing the pathological protein. Atomic force microscopy on artificial membranes containing interrupted and non-interrupted partial ATXN1 peptides revealed a different arrangement of the peptides within the lipid bilayer. Force-distance measurements indicated that membrane fragility increases with the lengthening of the uninterrupted glutamine. Transmembrane electrical measurements were performed on artificial bilayers and on the inner nuclear membrane of ATXN1 full length transfected cells. Both artificial lipid bilayers and cellular models demonstrated the dynamic appearance of ionic pathways. Uninterrupted polyglutamines showed not only a larger ionic flow, but also an increase in the single event conductance. Collectively, our results suggest that expanded ATXN1 may induce unregulated ionic pathways in the nuclear membrane, causing severe damage to the cell.

1. Introduction

Spinocerebellar ataxia type 1 (SCA1; OMIM ID: 164400) is an autosomal dominant cerebellar ataxia characterized by a progressive loss of motor coordination, speech impairment, and problems with swallowing. It is associated to a (CAG)n expansion in the SCA1 gene.

SCA1 is one of nine unrelated genes responsible for inherited diseases known as polyglutamine (polyQ) neurodegenerative disorders [1]. The mutational mechanism of these diseases is the expansion of a polymorphic CAG trinucleotide repeat that encodes a polyQ stretch in each causative gene. These disorders are Huntington disease (HD), spinal bulbar muscular atrophy (SBMA or Kennedy's disease), dentatorubropallidoluysian atrophy (DRPLA), and six dominantly inherited spinocerebellar ataxias (SCA1-3, SCA6, SCA7 and SCA17).

Abbreviations: SCA1, spinocerebellar ataxia type 1; ATXN1, ataxin 1; polyglutamine, polyQ; SBMA, spinal bulbar muscular atrophy; HD, Huntington disease; DRPLA, dentatorubropallidoluysian atrophy; NLS, nuclear localization signal; RBM17, RNA-binding motif protein 17; AFM, atomic force microscope

* Corresponding author at: Dipartimento di Biologia, Università degli Studi "Tor Vergata", Via della Ricerca Scientifica, 00133 Roma, Italy. Tel.: +39 0672594321; fax: +39 062023500.
E-mail address: carla.jodice@uniroma2.it (C. Jodice).

[1] LM, CC and DP contributed equally to this work.
[2] Present address: Dipartimento di Farmacologia, Università di Milano, Milano, Italy.
[3] Present address: Lab. of Experimental Endocrinology, Istituto Auxologico Italiano IRCCS, Milan, Italy.
[4] These authors should be regarded as Senior Authors.

0925-4439/$ – see front matter © 2012 Elsevier B.V. All rights reserved.
doi:10.1016/j.bbadis.2012.01.016

Normal SCA1 alleles contain from 6 to 45 CAG repeats, with those greater than 21 being always interrupted with 1–3 CAT trinucleotides [2–4]. By contrast, disease alleles are pure CAG tracts ranging from 39 to 82 units. The length of the repeat tract is a major contributor to the age of disease onset [5,6]. Typically the onset in individuals carrying a mutant SCA1 allele (40–50 repeats) is in their forties or fifties, but individuals with >70 repeat units have a juvenile form of SCA1 and show symptoms starting as early as the age of ten. By the age of sixty disease penetrance is essentially complete (for a review see [7,8]).

SCA1 encodes for a protein, ataxin 1 (ATXN1), that localizes in the nucleus through a functional nuclear localization signal (NLS) [9]. Inactivation of the NLS in an expanded ATXN1 results in a mutant protein that is no longer pathogenic [9]. This result, on the one hand, indicates that the ability of mutant ATXN1 to cause disease might be linked to its localization in the nucleus; on the other hand, it supports the conclusion that the toxicity of the expanded SCA1 allele is mediated at the protein level rather than at the RNA one.

Genetic studies have shown that expansion of the polyQ tract confers a toxic gain of function [10–15]. In particular, it seems unlikely that expansion of the polyQ eliminates ATXN1 normal function which is critical for Purkinje cells. In fact, mice lacking Atxn1 do not develop ataxia and Purkinje cell pathology [12]. On the other hand, these cerebellar disorders have been observed in mice overexpressing mutant ATXN1 [16] or knock-in mice expressing Atxn1 with an expanded polyglutamine tract [16]. However, the nature of this gain of function remains unexplained.

Although ATXN1 is widely expressed [17,18], mutant ATXN1 mainly causes neurodegeneration of cerebellar Purkinje cells, brain stem and spinal cord neurons. The selective neurotoxicity observed in SCA1 and other polyQ diseases, such as SBMA and HD, [19] could be due to protein domains outside the polyQ tract which play an important role in making the polyQ tract expansion necessary but not sufficient to cause pathology. In fact, evidence has been reported about the loss of function resulting from a defective interaction between expanded ATXN1 and specific proteins [9,20–24]. In particular, it has been shown that ATXN1 interacts with the RNA-binding motif protein 17 (RBM17) in a Ser776 and polyQ length-dependent fashion [25]. However, recently it has been found that ATXN1[30Q] with Ser776 replaced by Asp induces disease in Purkinje cells of transgenic mice as ATXN1[82Q], but fails to progress into neuronal degeneration [26].

It has been proposed that one of the mechanisms responsible for neuronal degeneration could involve the ability of isolated polyQ tracts to form large non-selective ion channels in planar lipid bilayers [27,28]. Moreover, when polyQ expansions are part of specific proteins, such as the huntingtin N-terminal fragment (htt1-89), they favor the association with phospholipids and membrane insertion [29].

In an effort to address the question whether polyQs, and more specifically expanded ATXN1, are prone to form anomalous membrane associations, we decided to analyze the effects of the expanded polyQ ATXN1 on the nuclear membrane. The analyses have been carried out *in vitro* and *in vivo* by comparing the results of various experiments performed with both normal ATXN1 variants, containing 31 and 45 repeats of glutamines interrupted by residues of histidine (31Q(H) and 45Q(H)), and pathological variants, containing 45 and 76 repeated glutamines (45Q and 76Q).

This research was carried out using a multidisciplinary approach. Electrophysiological experiments provided evidence that the interaction of uninterrupted partial ATXN1 peptide (pATXN1-Q) with artificial lipid bilayers causes a much higher increase of ionic membrane conductance with respect to interrupted partial ATXN1 peptide (pATXN1-QH). Force-distance curves measured by using the atomic force microscope (AFM) showed that the presence of polyQ tracts causes a decrease of the mechanical resistance of artificial lipid bilayers. This effect was much more pronounced for pATXN1-Q. Further experiments were performed with full length ATXN1 protein. We applied single channel recording on the inner nuclear membrane of ataxin-1 full length transfected cells. The pathological form (45Q in the present case) caused multiple ionic conductance compared to paucity of current levels of polyQ(H). Furthermore, the conductance induced by polyQ was modulated by Ca^{++} concentration, whereas it was practically insensitive to Ca^{++} concentration in the presence of polyQ(H). Finally, both electron microscopy and confocal images showed severe damage in the nuclear envelope of cells expressing expanded ATXN1-Q. In contrast, nuclei of cells transfected with non-pathological ATXN1 displayed a less extended damage to the membrane.

All these sets of data support the idea that uninterrupted expanded polyQs, either analyzed as recombinant peptides or as a full length protein, are able to insert themselves into lipid membranes causing both conductance increase and membrane destabilization. Due to the significant interplay between the inner nuclear membrane and the heterochromatin stabilization [30,31], we suggest that the progressive and inexorable degeneration caused by polyglutamine disorders derives from the nuclear envelope loss of function.

2. Materials and methods

2.1. Plasmids and polypeptides preparation

Constructs expressing partial ATXN1 peptides, whose sequences are: pATXN1-32Q(H) → aa_{34}-Q_{14}HQHQ$_{15}$-aa_{47}; pATXN-45Q(H) → aa_{34}-Q_{12}HQHQ$_{12}$HQHQ$_{15}$-aa_{47}; pATXN-45Q → aa_{34}-Q_{45}-aa_{47} and pATXN-76Q → aa_{34}-Q_{76}-aa_{47}, have been described [2].

Escherichia coli BL21 carrying the pGEX expression plasmids of interest were grown to an O.D.600 of 0.6–1.0 at 30 °C (the low incubation temperature reduces the level of instability), and induced with IPTG [1 mM pGEX-poly32Q(H), pGEXpoly45Q(H) and pGEX-poly45Q, and 0.1 mM pGEX-poly76Q] for 3.5 h as described by the manufacturer (Amersham-Pharmacia). Cultures (30 ml) of induced bacteria were centrifuged for 15 min, and the resulting pellets were resuspended in 1.5 ml of lysis buffer [phosphate buffered saline (PBS) 1×] containing 0.1 mg/ml lysozyme and 0.01 mg/ml DNase I, and stored overnight at −20 °C. Cells were lysated with 10 freeze/thaw cycles, and the resulting lysates were clarified by centrifugation in a microfuge at 13,000 rpm for 10 min. Cleared lysates were incubated overnight at 4 °C with 100 μl of a 50% slur of glutathione sepharose 4B. The beads were washed three times and resuspended in lysis buffer (PBS 1×). The bound GST-polyQ fusion proteins were eluted with 100 μl of glutathione elution buffer (10 mM reduced glutathione). Protein concentrations were determined by the Bio-Rad (Germany) dye binding assay using bovine serum albumin as standard.

Full-length ATXN1 cDNAs containing 32Q(H), -45Q(H), 45Q and 76Q(H) polyglutamine stretches were cloned in both pEGFP-N3 and pIRES2-EGFP (Clontech) plasmids for expression in mammalian cells.

2.2. Transfection and immunocytochemistry

COS1 cell lines were maintained in Dulbecco's minimal essential medium (DMEM) enriched with 10% fetal calf serum (FCS). Transient transfection experiments were performed in 60 mm plates using 1 μg of DNA combined with DNA Plus and Lipofectamine reagents. Cells were fixed with 4% paraformaldehyde and/or lysed with PBS supplied with 0.2% Triton-X 100, 48 h post-transfection. For immunocytochemical labeling, cells were cultured on glass coverslips. Forty-eight hours post-transfection, cells expressing the EGFP-ATXN1 fusion proteins were washed once with 1× phosphate buffered saline (PBS) and fixed in 4% paraformaldehyde for 15 min. The cover slips were mounted on slides and the cells were visualized using a

fluorescent microscope with the appropriate GFP filter (GFP fluorescence is excited at 488 nm and its emission examined at 516 nm). Immunodetection of emerin was done using a polyclonal antibody against emerin (kindly supplied by Dr. Toniolo; [32]) at 1:100.

2.3. Quantification of aggregate formation and abnormal cell nuclei

Aggregate formation and nuclear morphology were assessed using a fluorescence microscope. For each type of transfection, more than 400 EGFP-positive COS1 cells were selected and the proportion of cells with abnormal nuclei and/or aggregates was counted, as well as the size of the aggregates themselves. Cells were considered abnormal if the DAPI-stained nuclei showed apoptotic morphology (fragmentation or pyknosis) [33] and absence of total overlap between the normal ATXN1 localization in the nucleus (green fluorescence) and the chromatin material (DAPI staining).

2.4. Transmission electron microscopy

Transmission electron microscopy analysis was undertaken on transfected COS1 cells with pEGFP-ATXN1-32Q(H), -45Q(H), 45Q and 76Q(H), as well as empty pEGFP-N3 as control. Cells were fixed with 2.5% glutaraldehyde in 0.1 M cacodylate buffer for 1 h at 4 °C. Post fixation was performed with 1% OsO4. Samples were then dehydrated in a graded ethanol series and embedded in Spurr resin. Ultrathin sections were stained with 2% uranyl acetate and observed under a Zeiss EM900 transmission electron microscope. Images were captured digitally with a Mega View II digital camera (SIS).

2.5. Preparation of supported lipid bilayers

Unilamellar vesicles containing pATXN1 peptides embedded in the membrane were obtained by hydrating a mixture of diphytanoyl-phosphatidylcholine and pATXN1-31Q(H), -45Q(H), or -45Q. The lipid concentration was 1.2 mM, while the protein concentration was 1.5 nM. The hydration process was performed at room temperature in distilled water, with the aid of an ultrasonic bath (ACAD, Genoa, Italy) for 10 min. Then the sample was sonicated with a tip sonicator (Ultrasonics Ltd., Northants, UK) for 40 min; to prevent overheating the sample was immersed in a water bath kept at 20 °C. To remove large lipid aggregates and titanium impurities released by the tip, the suspension was centrifuged for 10 min at 11,500 ×g in a Sorvall RC-SB Superspeed Centrifuge (Du Pont Instruments, Newton, CT). Supported lipid bilayers were prepared via vesicle fusion on freshly cleaved mica substrates. The liposome solution was incubated on the mica surface at room temperature for 1.0 h; then the sample was rinsed and allowed to equilibrate for 2 h. All the AFM experiments were performed in distilled water.

2.6. Atomic force microscopy

AFM experiments were carried out using a NanoWizard II system (JPK Instruments, Berlin, Germany), working under distilled water at room temperature. V-shaped standard silicon nitride cantilevers with a nominal spring constant of 0.32 N/m (NP, Veeco, Woodbury, NY; US) were used both for imaging and bilayers rupture force measurements. Images were collected working in tapping mode to minimize the lateral force applied to the sample during scanning. Typical scan rates were between 0.5 and 1.5 Hz. The drive amplitude was set between 0.6 and 1.5 V to induce a free amplitude oscillation of 0.7 V RMS. The tip resonance frequency was in the range between 10 and 12 kHz. Due to tip size effects, which cause an apparent increase of the size of the imaged object in the image plane, island widths measured from AFM images are overestimated as compared to the real ones. To evaluate the expected width, w, we used the equation $w = w_{meas} + 2h - 2\sqrt{h^2 + 2Rh}$ where w_{meas} is the measured island width, h is the measured island height and R the AFM tip radius.

To obtain the breakthrough force the spring constant of each cantilever was determined *in situ* before and after every experiment, using the thermal noise method [34]. The indenting speed was maintained constant to 1 μm/s in all the experiments to avoid any effect of the speed when comparing the bilayer rupture forces. The experiments were performed on at least three different samples for each protein species. For each single experiment 150–300 force curves were collected, indenting the bilayer in different positions. A custom routine for force curve analysis working in MatLab environment was developed [35] the software automatically detects the yielding force for each single curve and displays the result graphically as shown in Fig. 4A.

2.7. Electrophysiological assay

Single-channel recordings from lipid bilayer were obtained by using the Tip–Dip method. In brief, patch clamp pipettes (Garner Glass 7052) were made using a P97 Sutter Instruments puller (Novato, CA), coated with Sylgard (Dow Corning, Midland, MI) and fire-polished to a tip diameter of 1–1.5 μm and 5–7 MΩ resistance. As soon as the pipette tip reached the bath solution, a 1,2-diphytanoyl-sn-glycero-3-phosphocholine (Diph-PC, Avanti Polar Lipids, Inc., Birmingham, AL) monolayer was spread on the surface. The electrode was repeatedly passed through the surface of the bath chamber solution until the pipette resistance rose above 5 GΩ. The lipid bilayer was regularly tested for a period of 10–15 min to search for unspecific electric current. An Axopatch 1D amplifier and pClamp 8 (both from Molecular Device, Novato, CA) were used to record and analyze the single-channel currents. Current recordings were digitized at 5 kHz and filtered at 1000 Hz.

In almost all the experiments the same buffer was employed in the two compartments. The “trans” and “cis” solutions were 144 mM KCl, 0.1 mM CaCl2, 1.2 mM MgCl2, 1.1 EGTA, 10 mM Hepes, and pH 6.2. Occasionally to check membrane selectivity the “trans” solution adopted was 144 mM NaCl, 1.8 mM CaCl2, 1.2 mM MgCl2, 10 mM Hepes, and pH 7.0. Membrane voltages (Vm) and ion currents were relative to the solution inside the glass pipette: as an example, an inward current is defined as a cation moving from the electrode to the bath chamber.

Purified Ataxin-1 proteins employed in Tip–Dip assays were made up to a final concentration of approximately 20 nM in a solution containing: 144 mM KCl, 0.1 mM $CaCl_2$, 1.2 mM $MgCl_2$, 1.1 EGTA, 10 mM Hepes, pH 6.2 and DMSO 55%. Two microliters of this solution was added to 1 ml of the test solution.

Patch clamp electrophysiology was performed in cell-attached configuration on nuclear inner membrane. Nuclei were isolated by centrifugation sequences on a sucrose gradient starting from a cell homogenate and then exposed for 1 h to a 1% Citrate containing solution. According to an old procedure [36] revisited by Gilchrist and colleagues [37], purification of nuclei in citrate-containing buffers leads to preferential removal of the outer nuclear membrane.

GFP fluorescence, detected by a Zeiss Axiovert 100 fluorescent microscope, allowed recognition of transfected nuclei for electrophysiological experiments. The bath solution was (in mM): 144 KCl, 0.1 $CaCl_2$, 1.2 $MgCl_2$, 1.1 EGTA, 10 Hepes, and pH 6.2. The cell-attached electrode was filled with the same solution. The Axopatch 200 B amplifier and pClamp 9 acquisition software (both from Molecular Device, Novato, CA) were used to record and analyze the single-channel. Current recordings were digitized at 5 kHz and filtered at 1000 Hz. The single channel conductance was determined by linear regression of the i/V relationships.

Data are presented as mean ± SEM. Values obtained from different experiments were tested for statistical differences using an

independent two population *t* test (Origin software; Origin Lab, Northampton, MA).

3. Results

In this study normal and pathological ATXN1 alleles have been employed. The normal allele 31Q(H) is one of the most frequent alleles in humans, while 45Q(H) is an uncommon allele containing 45 repeat units. Although the length of the latter is well within the range of expansions, two blocks of CAT-CAG-CAT interruptions (HQH at the protein level) suppress the pathological effects of the expansion [2,7]. The pathological alleles were represented by two expanded SCA1 containing 45 and 76 uninterrupted CAG repeat units (45Q and 76Q). It is worth noting that 45Q(H) and 45Q alleles are of the same length, but while the latter causes the disease, the former does not. These alleles represent a molecular model making it possible to discriminate between causative effects of pathogenic polyQ expansions and epiphenomena merely due to the length of the polyQ tract.

3.1. Aggregation and cell death in mammalian cells expressing normal and expanded ATXN1

COS1 cells were transfected with ATXN1 full length proteins containing 31Q(H), 45Q(H), 45Q or 76Q repeat segments fused to an enhanced fluorescent protein (EGFP). All these proteins are prone to form aggregates, but this feature increases with the repeat length. In fact, we found that the majority of COS1 cells transfected with normal ATXN1-31Q(H) showed a diffuse staining accompanied by many small aggregates; by contrast, cells transfected with mutant ATXN1-76Q contained fewer nuclear aggregates much larger in size, matching previous data from similar experiments [38]. The images obtained from cells transiently transfected with ATXN1-45Q showed an intermediate behavior, characterized by many cells with a diffuse staining of the nucleus accompanied by large aggregates. Interestingly, results obtained from cells transfected with ATXN1-45Q(H) were very similar to those obtained with ATXN1-45Q (data not shown).

The toxicity of the four constructs was tested by morphological analysis of transiently transfected COS1 cells. Cells expressing polyQ presented a significantly higher frequency (chi square = 23.35; $P \ll 0.001$) of anomalous nuclei with respect to those expressing polyQ(H) (Fig. 1). Interestingly the two normal alleles, 31Q(H) and 45Q(H), produced similar results, thus supporting the hypothesis that the toxicity of polyQ stretches depends on the particular structure formed by pure glutamine repeats.

3.2. Morphological analyses of nuclear membrane

To investigate whether expanded ATXN1 interacts with the nuclear membrane we carried out an immunofluorescence study using a marker for the inner nuclear envelope. Emerin is a serine-rich inner nuclear membrane protein and a member of the nuclear lamina-associated protein family [39]. COS1 cells were transfected with vectors for the expression of the EGFP and fusion proteins of EGFP and full length ATXN1-31Q(H), -45Q(H), -45Q and -76Q. DAPI was used to detect nuclei while nuclear membranes were visualized by an anti-emerin antibody detected by a TRITC-conjugated secondary antibody (red). Cells transfected with EGFP showed a diffuse green color in the nucleus and the cytoplasm, most of them displaying the usual emerin localization at the nuclear membrane level. In contrast, all cells expressing EGFP/ATXN1 fusion proteins showed the green color to be limited to the nucleus, as expected because of the ATXN1 NLS (Fig. 2A); a large emerin loss surrounding the nucleus was observed in cells expressing ATXN1-45Q and 76Q.

The immunofluorescence results indirectly suggest that severe damage occurs in the nuclear membrane of cells expressing ATXN1-

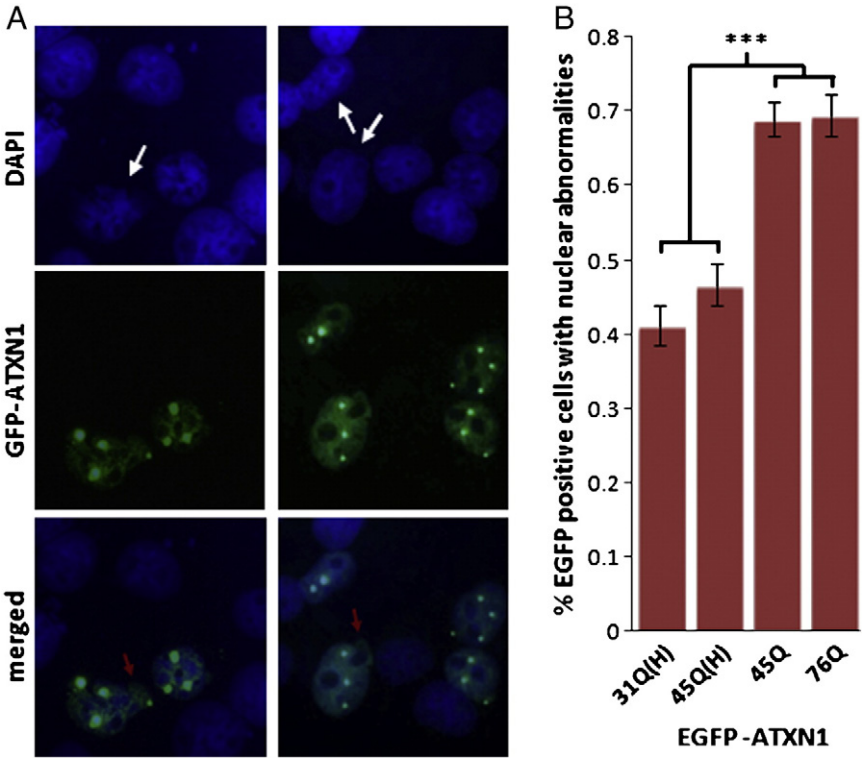

Fig. 1. Analysis of transiently transfected COS1 cells with ATXN1 full length proteins containing 31Q(H), 45Q(H), 45Q or 76Q repeat segments. Significantly stronger toxicity of polyQ stretches is observed as compared to polyQ(H). (A) Example of anomalous nuclei, showing pyknosis or fragmentation, indicated by white arrows. The pictures show cells stained with the nuclear dye DAPI (top row), cells expressing EGFP/ATXN1 (middle row) and merged images (bottom row). In the merged panels, note the green fluorescence coming out of the nucleus (blue stain) indicated by the red arrows. This suggests a nuclear envelope leakage. (B) Percentages of transfected COS1 cells showing marked abnormal nuclear morphology after 48 h. $^{***}P \lll 0.01$.

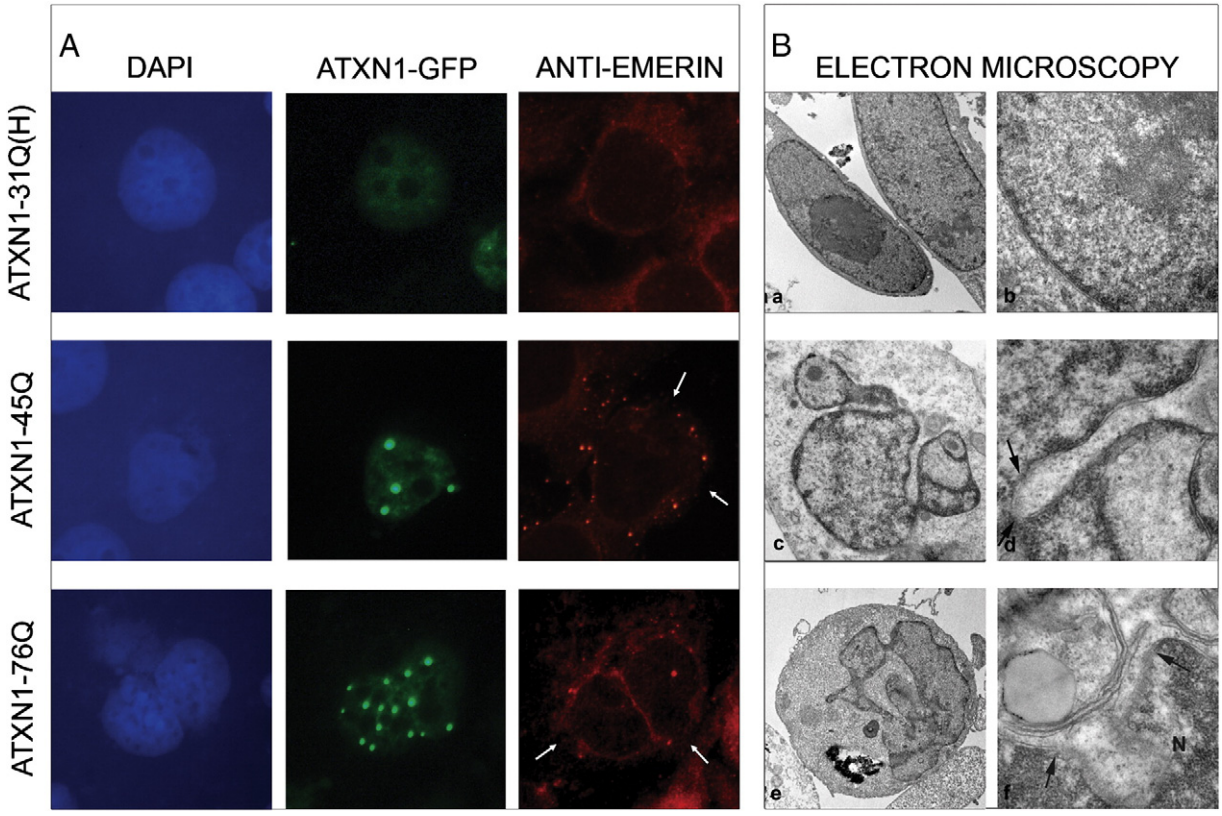

Fig. 2. Cells expressing expanded ATXN1 show a marked damage of the nuclear envelop. COS1 cells were transfected with pEGFP/ATXN1 fusion proteins containing 31Q(H), 45Q or 76Q repeat segments (Panels A). After 48 h they were fixed and stained with anti-emerin (red fluorescence). Arrows indicate transfected cells showing loss of emerin. Transmission electron micrographs (Panels B) showing the ultrastructure of COS1 cells transfected with ATXN1-31Q(H), or ATXN1 proteins containing 45Q or 76Q repeat segments. Cells expressing ATXN1-31Q(H) (a, b) show normal appearance with oval shaped nuclei and intact nuclear double membrane (b). Cells transfected with expanded ATXN1-45Q (c, d) display changes of nuclear morphology characterized by profound invaginations and nuclear indentations (arrows) (d). In cells transfected with expanded ATXN1-76Q (e, f) abnormalities consist in deeply convoluted nuclear profile with breakages into the nuclear envelope (arrows) (f). N = nucleus. Original magnifications: (a, e) 7000×; (b) 30000×; (c) 20000×; (d, f) 50000×.

45Q and 76Q. For a deeper insight into the nuclear membranes, we also analyzed these cells with electron microscopy (Fig. 2B). Profound invaginations and discontinuities of the nuclear envelope were observed in a large number of COS1 cells expressing ATXN1-45Q and 76Q. Overall, these results suggest a toxic action of expanded polyglutamines on the membranes.

3.3. Mechanical properties of artificial membranes in the presence of different forms of partial ATXN1 peptides

To model the interaction between ATXN1 and the nuclear membrane, we performed experiments on artificial bilayers containing uninterrupted or interrupted partial ATXN1 peptides. The latter were mixed with the lipids before membrane preparation. AFM inspection of the pATXN1 variants before mixing with the lipids showed the presence of bead-like structures which can be identified with monomers and oligomers (not shown). The mean height of these structures is 1.2 ± 0.1 nm for pATXN1-32Q(H), 1.9 ± 0.1 nm for pATXN1-45Q(H) and 1.8 ± 0.1 nm for pATXN1-45Q. Taking into account the very low concentration of pATXN1 peptides in the membrane (2 nM), it is likely that most of the peptides remained in the monomeric or at most in the oligomeric state.

Liposomes containing pATXN1-31Q(H), -45Q(H) or -45Q were deposited on freshly cleaved mica to form self-assembled planar bilayers. These have been imaged using tapping mode AFM. In membranes containing pATXN1-45Q(H) and -45Q round-shaped islands are visible (Fig. 3A, B). The islands observed for pATXN1-45Q(H) and -45Q have different features. In particular, for pATXN1-45Q most of the structures observed are islands whose diameter was 32 ± 7 nm. These islands do not protrude from the membrane surface; therefore their size is not influenced by AFM tip effects (Fig. 3A). A different behavior is observed in membranes containing pATXN1-45Q(H). In this case round-shaped objects protruding from the membrane are visible (Fig. 3A, inset). Their apparent diameter is 11 ± 4 nm and their height with respect to the membrane surface is 0.50 ± 0.06 nm. As these objects protrude from the membrane surface, their size in the scan plane is affected by the AFM tip size. Correction factors are discussed in the "Materials and methods" section; taking into account the correction factor, the real object size is in the order of a few nanometers. The difference between islands formed by pATXN1-45Q and pATXN1-45Q(H) is evidenced by tapping mode phase imaging. In fact, islands associated to pATXN1-45Q display very different mechanical properties compared to the membrane in which they are embedded (Fig. 3B). Conversely, from a mechanical point of view, islands associated to pATXN1-45Q(H) cannot be distinguished from the background (Fig. 3B, inset). Fig. 3D compares island profiles measured in the two cases from cross sections of the corresponding topographic AFM images. Membranes containing pATXN1-31Q(H) showed a behavior similar to those with pATXN1-45Q(H). Round-shaped islands were observed protruding from the membrane, with a height of 0.6 ± 0.1 nm and an apparent diameter of 18 ± 3 nm (results not shown).

Round-shaped islands are absent in pure lipid membranes (Fig. 4D); in addition, the islands are homogenous in shape and size. This suggests that they can be identified as protein or protein–lipid complexes inserted in the membrane. We found a different behavior for non-pathological and pathological peptides, with islands protruding from the membrane in the former case and completely embedded

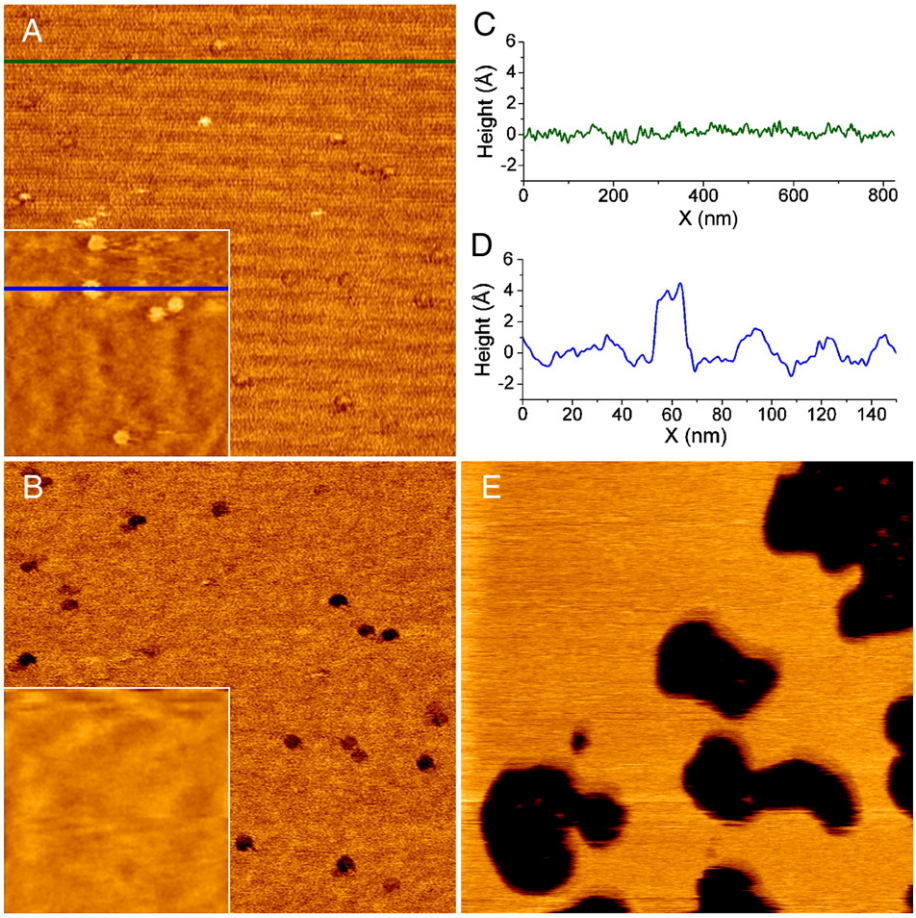

Fig. 3. Tapping mode AFM images of artificial membranes containing pATXN1 peptides. (A) Topographic image of a membrane containing pATXN1-45Q. Inset: topographic image of a membrane containing pATXN1-45Q(H). (B) Phase images of the same regions reported in (A). (C) Height profile obtained for the membrane containing pATXN1-45Q, showing that islands do not protrude from the background. (D) Height profile obtained for the membrane containing pATXN1-45Q(H) and showing an island protruding from the background. Profiles (C) and (D) were obtained from the image sections traced along the green line in (A) and blue line in inset (A) respectively. (E) topographic image of a pure lipid membrane. Scan size (A), (B), (E), 830 nm; insets, 160 nm. Z range (A) and inset (A), 3.0 nm; (E), 8.0 nm.

in the membrane in the latter. This is a further piece of evidence supporting the conclusion that islands are indeed protein or lipid–protein complexes, and is in agreement with the electrophysiological experiments reported in the next section, showing a different membrane permeabilization induced by pathological and non-pathological peptides.

While imaging of pure lipid membranes and membranes containing pATXN1-31Q(H) was easily achieved, obtaining images of membranes with pATXN1-45Q(H) was more difficult; indeed, in the case of membranes with pATXN1-45Q it was extremely difficult, suggesting an increased instability of the system as the peptide toxicity is increased. To quantify this behavior, we performed force-distance measurements to obtain the force required to penetrate the membrane with the AFM tip. This measurement made it possible to obtain information about the mechanical resistance of the membrane; the lower the penetration force, the more fragile is the membrane. Fig. 4A shows a typical force-distance curve measured as the tip gradually approaches the supported membrane. When the tip is far from the surface, no interaction occurs; this corresponds to the horizontal region in the curve of Fig. 4A. The linear region corresponds to contact between tip and sample, resulting in a cantilever deflection, and therefore the interaction force, proportional to the sample advancement. When the force reaches a critical value, the tip penetrates the membrane; such a yielding force is indicated by the double arrow in Fig. 4A. Membrane penetration corresponds to a sudden force decrease in the force-distance curve. The distributions of yielding forces for pure lipid membranes and membranes containing different pATXN1 peptides are reported in Fig. 4B–E. Interestingly, the distribution of yielding forces for membranes containing pATXN1-31Q(H) is shifted towards lower values as compared to that of the pure lipid. A further shift is observed for membranes containing pATXN1-45Q(H), while the largest shift occurs for membranes containing pATXN1-45Q. These results indicate that membrane destabilization increases as the peptide toxicity is increased.

3.4. Electrical properties of artificial and biological membranes in the presence of different forms of polyQ expanded ATXN1

The results of the experiments on the mechanical properties of lipid bilayers exposed to pATXN1 peptides clearly suggest that these peptides are able to interact with biological membranes. The nature of this interaction appears to be functional as well as structural. The bilayer mechanical parameters are affected by the number of glutamine repeats in the protein under observation. The more expanded are the polyQ tails interacting with the bilayer, the more fragile is the membrane (Fig. 4). From the functional point of view, this result suggests that membranes interacting with a higher number of glutamine repeats should have a lower electrical resistance and, consequently, be more permeable to ions. Fig. 5 presents measurements of membrane permeability obtained in artificial membranes containing different types of expanded pATXN1 peptides, clamped to 80 mV. As in AFM experiments, the peptides were mixed with the lipids

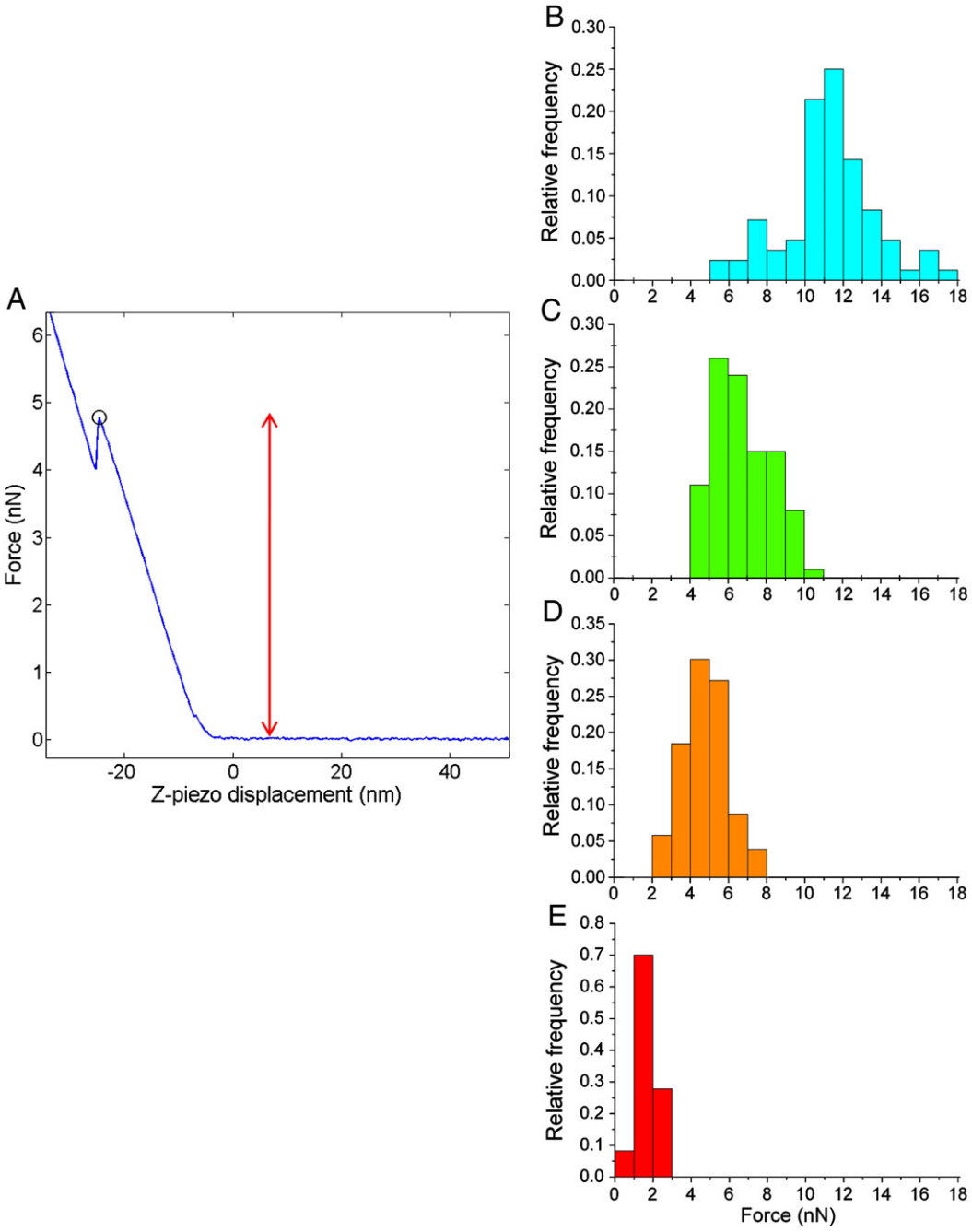

Fig. 4. (A) Typical force-distance curve measured on a supported lipid membrane. The horizontal region corresponds to absence of interaction between the AFM tip and the sample. In the linear region the interaction between tip and sample increases with the tip advancement. The jump in the curve indicates membrane penetration; the corresponding yielding force is indicated by the double arrow. (B–E) Distributions of yielding forces showing that the mean yielding force of artificial membranes containing pATXN1 peptides decreases as the peptide toxicity is increased. (B) Pure lipid bilayers; (C–E) bilayers containing (C) pATXN1-31Q(H), (D) pATXN1-45Q(H), (E) pATXN1-45Q.

before membrane preparation. Tip Dip electrical recordings reported in Panel A clearly show higher activity for pATXN1-45Q and -76Q compared to pATXN1-31Q(H) and pATXN1-45Q(H). The electrical activity was quantified by analyzing the number of current levels for the different polyQ types. It is evident from Fig. 5A that a higher number of glutamine repeats correspond to a higher number of current levels. This is even more evident in the amplitude histograms plotted in Fig. 5B: pATXN1-45Q and -76Q plots show a larger number of events and display higher amplitudes compared to pATXN1-31Q(H) and -45Q(H). This higher activity results in enhanced membrane permeability, as shown by current/voltage plots in Fig. 5C. The slope of the i/V curves increases progressively from pATXN1-31Q(H) to -76Q. Interestingly, a large difference in conductance is undoubtedly visible between the histidine-interrupted and uninterrupted peptides. In particular, lipid membranes containing pATXN1-45Q show an average conductance whose value is almost double compared to those with the histidine interrupted form.

The results presented above suggest that polyQ chains are able to lower the bilayer electrical resistance. Furthermore, the longer the polyQ tail, the lower appears the membrane resistance. The immunostain experiments (Fig. 2) show that in transfected COS1 cells, ATXN1 accumulates in the nucleoplasm. Co-localization experiments suggest a close relationship between polyQ proteins and the nuclear inner membrane (Fig. 2). This raises the question whether there is a functional interaction between the internal membrane of the envelope and polyQ proteins. After 48 h from the transfection using pIRES-

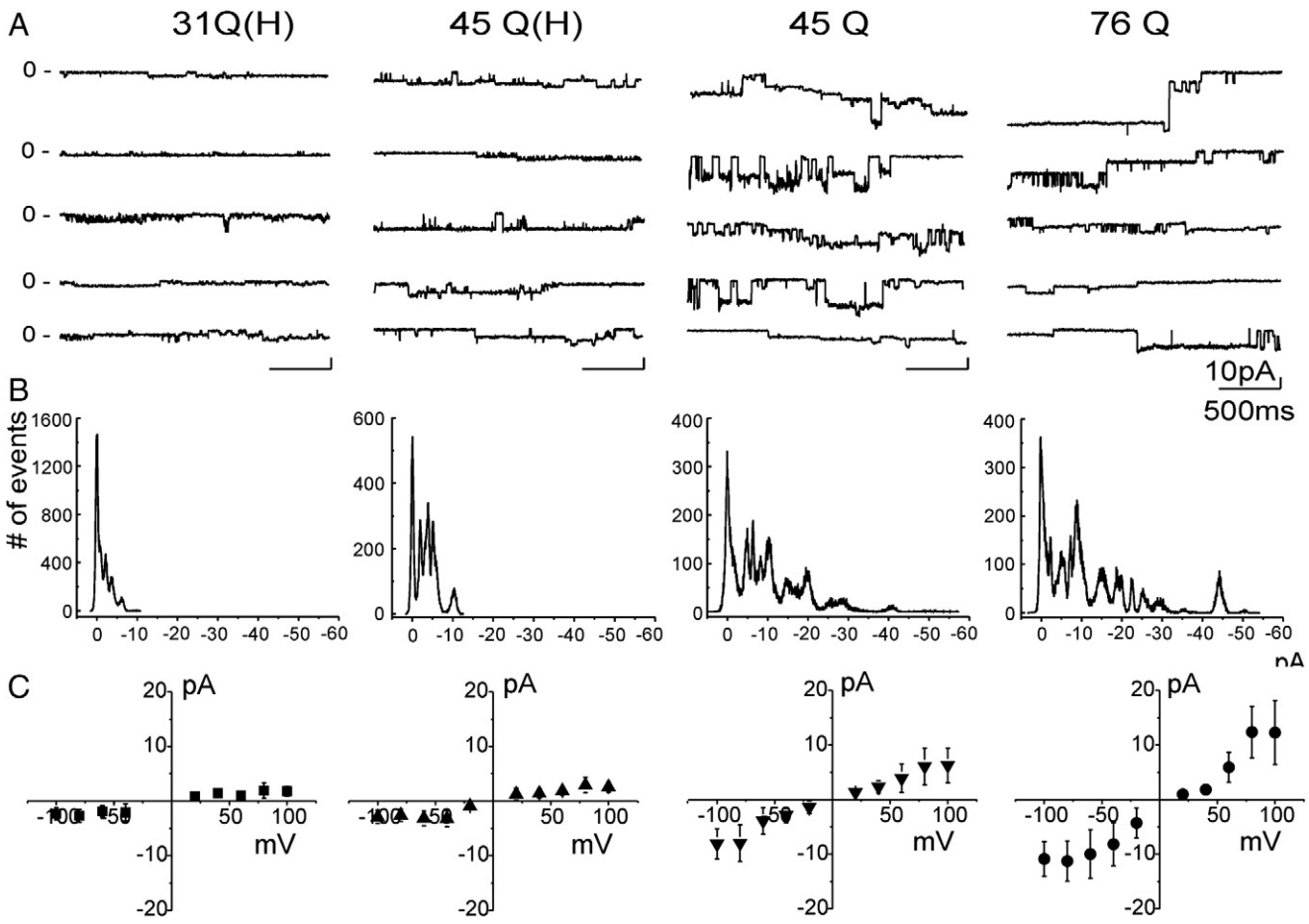

Fig. 5. Electrical behavior of artificial membranes containing different pATXN1 peptides. (A) Current traces recorded at 100 mV membrane potential in Tip Dip experiments using artificial lipid bilayers containing 20 nM of the indicated pATXN1 peptide. (B) Amplitude histograms of the corresponding current levels. Larger current levels are measured for the uninterrupted peptides. The current/voltage relationships in (C) show the averages of 20 current recordings at 10 different test potential for each polyQ type.

ATXN1-45Q(H) and -45Q plasmids, COS1 cells expressing the full length recombinant ATXN1 proteins were identified by GFP fluorescence. Cell nuclei were isolated and the outer membrane was gently removed by a chemical treatment (see Materials and methods for details). This procedure eliminated the external membrane of the nuclear envelope on 90% of the total nuclei surface. At the top of Fig. 6 we show electron microscopy pictures of isolated nuclei in control conditions (A) and after the removal of the outer membrane (B). Ultrastructure of pIRES-ATXN1-31Q(H) and -45Q(H) transfected nuclei was substantially similar. The possibility to test 76Q polyQ transfected COS1 nuclei was hampered by the paucity of living cells after 24–48 h from the transfection. What is intriguing is the comparison between consecutive and interrupted polyQ with the same number of repeats, such as the 45Q(H) and 45Q constructs, which showed a significant difference in toxicity experiments (Fig. 1). Patch clamp measurements on both preparations yielded single-channel recordings which confirmed the data previously described in Tip Dip experiments. Fig. 6 clearly shows a higher number of current levels in 45Q transfected nuclei compared to 45Q(H). The amplitude histograms plotted in Fig. 6C depict a number of current peaks doubled for 45Q compared to 45Q(H). Membrane interaction of the uninterrupted ATXN1 protein not only prompted a higher number of current levels, but also showed a larger amplitude of the single current level compared to the 45Q(H). To further characterize these patch recordings, we analyzed the current traces in more detail. We measured and averaged the amplitude of each single current level at the different membrane potentials applied. Fig. 7 shows examples of single channel recordings at +80 mV membrane voltage. The values of single current steps at the same potential were in general homogeneous, mainly at the beginning of the experiment. The bottom of Fig. 7 depicts i/V relationships for the average current levels using each recombinant protein type ($n=4$). On the left side, fitting the experimental current values at different membrane potentials resulted in a conductance slope of 11.0 ± 0.3 pS relative to 45Q(H) polyQ proteins. On the right, the calculated average conductance for 45Q protein is 25.0 ± 0.7 pS.

The difference in conductance could reflect a difference in ionic selectivity. However, the membrane current pathways show the same permeability to sodium, potassium or chloride (data not shown). Thus, monovalent ions are not discriminated by the permeability caused by the polyQ interaction with the biological membranes. By contrast, divalent ions act differently in the presence of 45Q(H) and 45Q. While histidine-interrupted polyQs are virtually insensitive to different calcium concentrations, 45Q exhibits a conductance depending on the divalent ion concentration. Fig. 8A shows two i/V curves from 5 different single-channel recordings. The linear regression curves of the current values obtained from nuclei transfected with the 45Q(H) protein at two different calcium concentrations (Fig. 8A left) are virtually coincident ($n=5$, t test $p<0.0001$). The conductance in low and high calcium concentration was 12 ± 2 pS and 12 ± 1 pS, respectively. However, in nuclei of cells transfected with the 45Q construct, the single current levels increased in amplitude following the increase of calcium concentration. The conductance changed from 23 ± 2 pS in 1.8 mM calcium to 32 ± 1 pS in 10 mM calcium (Fig. 8A right; $n=5$, $p<0.0006$). Examples of current recordings in the two different experimental conditions are shown in Fig. 8B. The histograms in Fig. 8C show that the average amplitude current levels are statistically different between 45Q and 45Q(H) in

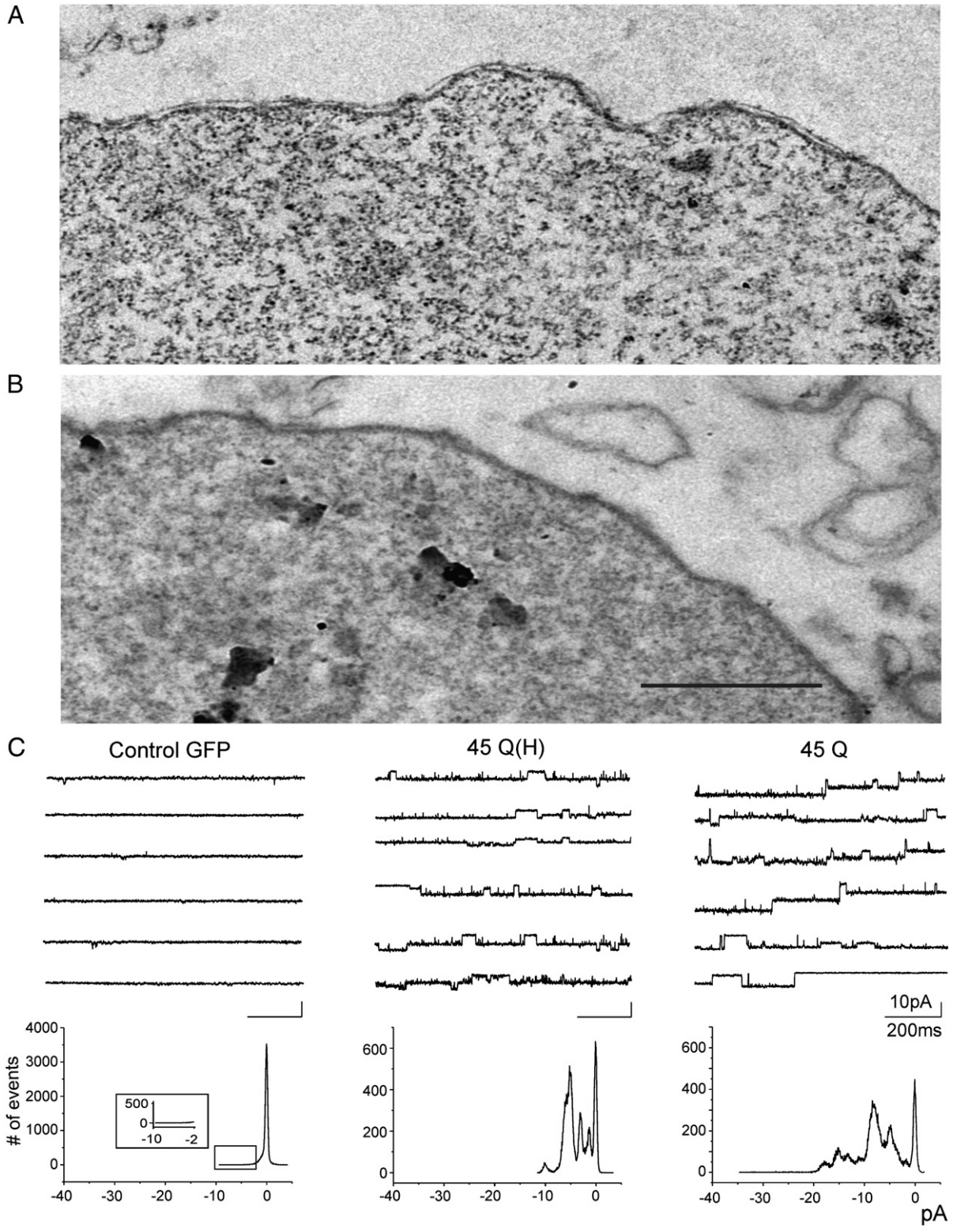

Fig. 6. Patch-clamp recordings on the inner nuclear membrane of COS1 cells transiently transfected with ATXN1 full length proteins. (A) Electron microscopy pictures of isolated nuclei and (B) nuclei treated for 1 h with Citrate to remove the outer membrane of the envelope. (C) Current recordings obtained on the inner nuclear membrane at −80 mV potential applied in the patch-pipette (top). Nuclei were isolated from control cells transfected with the GFP vector only (left), with 45Q(H) (center) and 45Q (right). At the bottom of panel C we show three examples of current amplitude distribution corresponding to the three different preparations. A total of 10 s continuous recording was analyzed at each membrane potential using a commercial software (see Materials and methods). Negative histogram peaks corresponding to the current levels visualized in the patch-clamp registrations above are completely absent in the control GFP (inset).

low calcium ($n = 5$, $p < 0.0001$). Furthermore, 45Q-transfected nuclei also showed a pronounced increase in the membrane conductance when the calcium concentration was raised to 10 mM ($n = 6$, $p < 0.0001$). Collectively, the electrophysiological measurements show that the conductance of 45Q(H) is insensitive to the calcium concentration. By contrast, 45Q not only shows a higher conductance

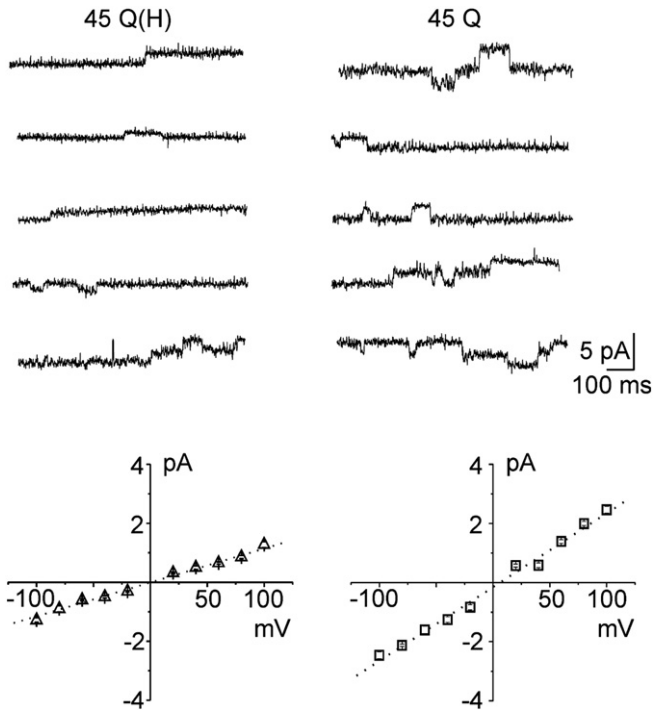

Fig. 7. Single event conductance obtained from current recordings on the inner nuclear membrane of COS1 cells transiently transfected with ATXN1 full length proteins. Current traces at 80 mV membrane voltage are shown in the top panels for interrupted (left) and 45Q (right). Corresponding current/voltage relationships are plotted at the bottom of the figure. The average conductance is 11.0 ± 0.3 pS for 45Q(H) and 25.0 ± 0.7 pS for 45Q.

in physiological calcium; but it also displays a significant conductance increase as the calcium concentration is increased. The ratio between average current levels measured for 45Q and 45Q(H) has similar values of 2.1 ± 0.2 for tip dip and 1.9 ± 0.1 for patch clamp experiments.

4. Discussion

Although the genetic basis of polyQ diseases, and more specifically of SCA1, was recognized about twenty years ago, their molecular basis is still controversial. Several issues are still open regarding the polyQ pathogenesis, in particular i) whether the specific structure of expanded polyQ results in toxicity to cells; ii) how the expanded polyQ proteins cause neurodegeneration. A number of proteins interact with ATXN1. Among these proteins there are several transcriptional regulators, including the corepressor SMRT (silencing mediator of retinoid and thyroid hormone receptors), Drosophila SENS (Senseless) and its mammalian homolog Gfi1 (growth factor-independent 1), the human homolog of the Drosophila repressor CIC (Capicua), and the RORα-Tip60 complex (reviewed in [1]). These data could suggest that mutant ATXN1 affects the normal regulation of the cell metabolism. Nevertheless, the neurodegeneration caused by expanded polyglutamines is a complex pathology and it is likely that more than one mechanism contribute to SCA1 disease.

Recently, Duvick et al. [26] showed that a SCA1-like disease in mice is induced by a single aminoacid substitution in ATXN1 protein disrupting a phosphorylation site. However, the point mutation failed to cause any neurodegenerative process. Cell death only occurred in the presence of an expanded polyQ tract. These results support a model in which the pathogenesis of SCA1 is based on at least two different molecular mechanisms, involving induction of disease in Purkinje cells on the one hand and neuronal degeneration on the other. The aim of our work is to gain new insight into the relation between expanded polyQs and neurodegeneration. To this purpose, we focused on the interaction between expanded ATXN1 and lipid membranes. We carried out experiments both on cellular models transfected with full length ATXN1 and on artificial lipid bilayers containing polyQ peptides. Although in these cellular models ATXN1 is overexpressed, transgenic mice carrying exogenous overexpressed expanded ATXN-1 recapitulate disease pathology with characteristic behavioral phenotypes [40], thus suggesting that overexpression does not alter the accumulation pathway.

We compared expanded pathological (polyQ) and interrupted (polyQ(H)) non-harmful polyglutamine tracts. In particular, we considered pathological and non-pathological ATXN1 variants of the same length. This allowed us to discriminate between toxic effects acquired by consecutive CAG repeats and epiphenomena due to the overall length of the expansion. In fact, ATXN1-45Q(H) is a normal form of the protein prone to forming nuclear aggregates at an extent comparable with the pathological ATXN1-45Q of the same length, when expressed in COS1. However, these two variants displayed a remarkable difference in toxicity (Fig. 1). It has been suggested that the ability of histidine insertion to suppress expanded polyQ toxicity does not lie in a reduced recruitment activity of the resulting amyloid aggregates [41], but rather in an altered pathway of spontaneous aggregation, still not clearly characterized *in vivo*. Thus, the reduced toxicity may derive, not from reduced aggregation rates, but because of some critical change in aggregate properties.

Due to the combination of polyQ ability to interact with membranes [27,28] and ATXN1 localization in the nucleus, it is expected that the pathological activity involves the inner nuclear membrane. Indeed immunofluorescence and electron microscope images of transfected cells showed a remarkable nuclear membrane disruption. The extent of this phenomenon is correlated with the number of uninterrupted glutamines (Fig. 2).

Atomic force microscopy images of artificial membranes showed a different arrangement of the interrupted and non-interrupted peptide within the lipid bilayer, indicating a deeper insertion of the pathological variant in the membrane. This gave rise to the formation of defects in the lipid film, which were also revealed by changes in the mechanical properties of the membrane. The longer the uninterrupted glutamine stretch, the more fragile was the membrane (Figs. 3 and 4).

The presence of transient defects in the membranes upon insertion of polyQ peptides was clearly shown by transmembrane electrical measurements. Both artificial lipid bilayers and cellular models demonstrated the dynamic appearance of ionic pathways. Uninterrupted polyQs showed not only a larger ionic flow, but also an increase in the single event conductance. This suggests the transient formation of larger membrane gaps.

It is well known that several misfolded proteins, even if unrelated in their primary sequence, are able to self-aggregate into a similar amyloid structure [42]. It has also been reported that the interaction of amyloids with biological membranes reduces the membrane electrical resistance [43–46]. In this work we show that polyQs, whether interrupted or not, exhibit single channel-like behavior both in artificial lipid bilayers (Fig. 5) and in cell nuclear membranes (Fig. 6). Hirakura and colleagues [27] calculated a conductance range of 19 to 220 pS for the polyQ non-selective channel in planar lipid bilayers. In Tip Dip experiments we found single current level conductance between 20 and 350 pS for pathological 45Q protein and between 20 and 550 pS for 76Q polyQ, while the range for non-pathological forms of ATXN1 (31Q(H) and 45Q(H)) was from 11 to 140 pS.

The conductance values resulting from cell-attached experiments on the inner nuclear membrane exhibit a much lower variability. Comparing current recordings of transfected COS1 cells, it is possible to calculate a single current level conductance of 11 pS for 45Q(H) and 25 pS for 45Q (Fig. 7). In addition, the non-pathological interrupted ATXN1 isoform induces not only lower conductance levels (Figs. 5 and 6), but also a reduced membrane fragility (Fig. 4) as

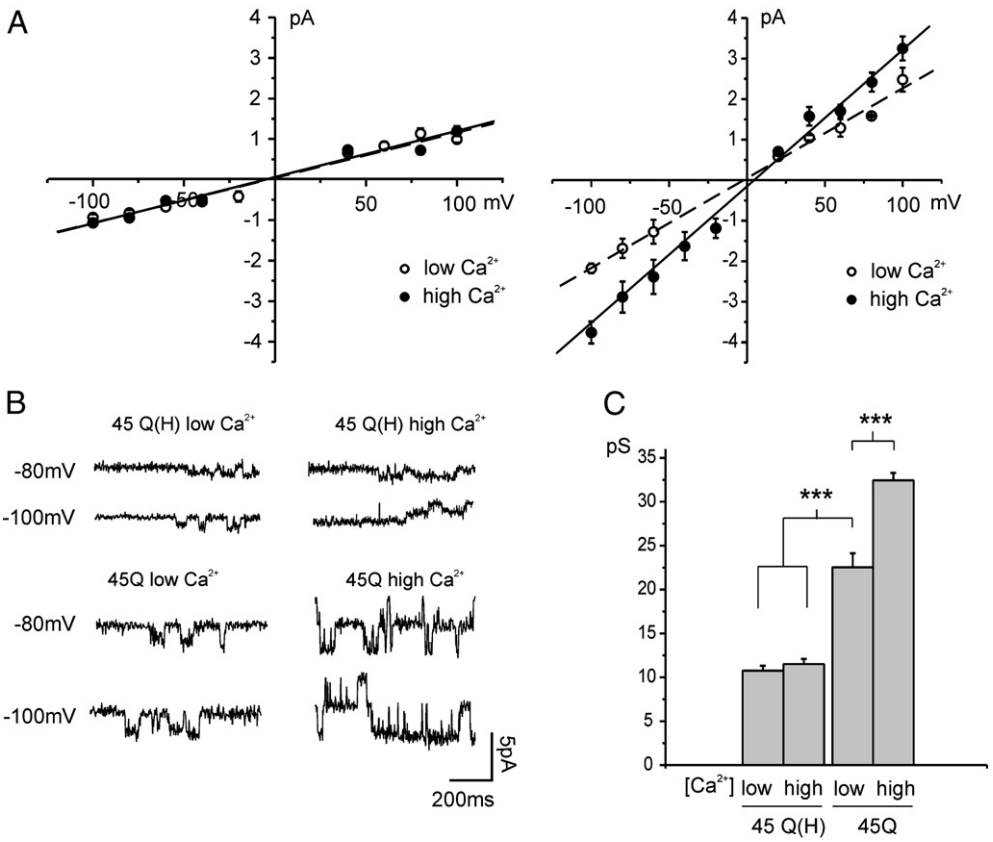

Fig. 8. Calcium ions permeability of the inner nuclear membrane of COS1 cells transiently transfected with ATXN1 full length proteins. (A) current/voltage relationships of patch-clamp current recordings in 1.8 and 10 mM $CaCl_2$ for 45Q(H) (left) and 45Q (right). The linear regression curves of the experimental points are superimposed in the case of 45Q(H) showing a similar conductance. By contrast, the calculated i/V conductance for 45(Q) shows different slopes for different calcium concentrations. (B) Individual current traces at two different test potentials showing that single current events are similar in low and high calcium for 45Q(H) (left) while they are markedly different for 45Q (right). (C) Comparison between conductance values obtained at different Calcium concentrations for 45Q(H) and 45Q. The histogram highlights the difference between 45Q and 45Q(H) in low calcium ($n=5$, $p<0.001$). 45Q-transfected nuclei in addition show a pronounced increase in the membrane conductance when the calcium concentration was raised to 10 mM ($n=6$, $p<0.001$).

compared to the pathological variant. The latter, besides showing a greater ability to permeabilize lipid bilayers (Figs. 5 and 6), is able to double the conductance of the single measurable event both in artificial as well as in biological membranes (Figs. 7 and 8). Since the ratio between average current levels measured for 45Q and 45Q(H) has similar values for both artificial bilayers and nuclear membranes, we suggest that the lipid composition does not play a crucial role in the ionic flow induced by the two ATXN1 variants. Collectively, our results from AFM and electrophysiological measurements suggest that these peptides cause transient bilayer defects, acting as unspecific ionic pathways. Whether a progressive permeabilization of the inner nuclear membrane represents an early event in the disease progression it is not clear. It is possible that change in conductance of the inner nuclear membrane is a parallel effect of the pathological phenotype insurgency. It appears well established that the disease exordium characterized by neuronal dysfunctions is distinct from the neurodegenerative process [26]. In this context, overproduction and nucleoplasm accumulation of misfolded ATXN1 certainly anticipate neuronal death.

Of note, in marked contrast with 45Q, 45Q(H) does not change its conductance value when the calcium concentration is changed (Fig. 8). On the basis of AFM images, we can speculate that this different behavior lies in the different 3D arrangement of the interrupted and uninterrupted polyQ in the membrane. The different permeability properties of the pathological and the non-pathological ATXN1 isoforms could certainly account for the different levels of cell toxicity showed in Fig. 1. It is expected that ATXN1 has a preferential interaction with the inner nuclear membrane due to preferential protein accumulation in the nucleoplasm [9]. Opening unregulated ionic pathways permeable to calcium in the inner nuclear membrane by uninterrupted polyQ is certainly dangerous for the genetic material structure and function, giving rise to progressive cellular damage.

All the results here described are consistent with the clinical observation of a negative correlation between the length of the expansion and both the age at onset and the duration of the disease. Uncovering the pathogenic mechanism underlying the disease opens up the possibility of designing a strategy to cure, or at least delay, the disease symptoms. The process that we have highlighted with our experiments demonstrates that the interaction between pathological molecules and the nuclear membrane is responsible for the end point of cell degeneration. It is likely that at this stage the cell damage cannot be recovered. To prevent the cell death it is crucial to interrupt the process before polyQs are accumulated within the nucleus, so avoiding their interaction with the inner membrane. Therefore, a therapy for recovery would be effective if it addresses the early stages of the neurodegenerative process.

Author contributions

Conceived and designed the experiments: AG, CJ, MM and AR. Performed the transfection and immunocytochemistry experiments and analyzed data: DP, VF and CJ. Performed the electron microscopy experiments and analyzed data: LF and MP. Performed the atomic force microscopy experiments and analyzed data: CC, AR and AG. Performed the electrophysiology assays and analyzed data: LM, SA, FG

and MM. Contributed constructs expressing partial or full length ataxin 1: DP, VF and CJ. Wrote the paper: AG, CJ, MM and AR.

Acknowledgements

We thank Silvia Torrassa for help in the preparation of unilamellar vesicles and Marco Jacono for help in the force curve analysis. This work was supported by the Italian Ministero dell'Istruzione, Università e Ricerca (PRIN 20083ERXWS and 20078RWJBN), Universities of Genoa, Milan and Rome "Tor Vergata" and by the Italian Ministero della Salute (Ricerca corrente e finalizzata).

References

[1] H.Y. Zoghbi, H.T. Orr, Pathogenic mechanisms of a polyglutamine-mediated neurodegenerative disease, spinocerebellar ataxia type 1, J. Biol. Chem. 284 (2009) 7425–7429.
[2] V. Calabresi, S. Guida, A. Servadio, C. Jodice, Phenotypic effects of expanded ataxin-1 polyglutamines with interruptions *in vitro*, Brain Res. Bull. 56 (2001) 337–342.
[3] M.Y. Chung, L.P. Ranum, L.A. Duvick, A. Servadio, H.Y. Zoghbi, H.T. Orr, Evidence for a mechanism predisposing to intergenerational CAG repeat instability in spinocerebellar ataxia type I, Nat. Genet. 5 (1993) 254–258.
[4] C. Jodice, B. Giovannone, V. Calabresi, M. Bellocchi, L. Terrenato, A. Novelletto, Population variation analysis at nine loci containing expressed trinucleotide repeats, Ann. Hum. Genet. 61 (1997) 425–438.
[5] C. Jodice, P. Malaspina, F. Persichetti, A. Novelletto, M. Spadaro, P. Giunti, C. Morocutti, L. Terrenato, A.E. Harding, M. Frontali, Effect of trinucleotide repeat length and parental sex on phenotypic variation in spinocerebellar ataxia I, Am. J. Hum. Genet. 54 (1994) 959–965.
[6] L.P. Ranum, M.Y. Chung, S. Banfi, A. Bryer, L.J. Schut, R. Ramesar, L.A. Duvick, A. McCall, S.H. Subramony, L. Goldfarb, C. Gomez, L.A. Sandkuijl, H.T. Orr, H.Y. Zoghbi, Molecular and clinical correlations in spinocerebellar ataxia type I: evidence for familial effects on the age at onset, Am. J. Hum. Genet. 55 (1994) 244–252.
[7] M. Frontali, A. Novelletto, G. Annesi, C. Jodice, CAG repeat instability, cryptic sequence variation and pathogeneticity: evidence from different loci, Philos. Trans. R. Soc. Lond., B, Biol. Sci. 354 (1999) 1089–1094.
[8] B.P. van de Warrenburg, H. Hendriks, A. Dürr, M.C. van Zuijlen, G. Stevanin, A. Camuzat, R.J. Sinke, A. Brice, B.P. Kremer, Age at onset variance analysis in spinocerebellar ataxias: a study in a Dutch-French cohort, Ann. Neurol. 57 (2005) 505–512.
[9] I.A. Klement, P.J. Skinner, M.D. Kaytor, H. Yi, S.M. Hersch, H.B. Clark, H.Y. Zoghbi, H.T. Orr, Ataxin-1 nuclear localization and aggregation: role in polyglutamine-induced disease in SCA1 transgenic mice, Cell 95 (1998) 41–53.
[10] M.P. Duyao, A.B. Auerbach, A. Ryan, F. Persichetti, G.T. Barnes, S.M. McNeil, P. Ge, J.P. Vonsattel, J.F. Gusella, A.L. Joyner, M.E. MacDonald, Inactivation of the mouse Huntington's disease gene homolog Hdh, Science 269 (1995) 407–410.
[11] H. Ikeda, M. Yamaguchi, S. Sugai, Y. Aze, S. Narumiya, A. Kakizuka, Expanded polyglutamine in the Machado–Joseph disease protein induces cell death in vitro and *in vivo*, Nat. Genet. 13 (1996) 196–202.
[12] A. Matilla, E.D. Roberson, S. Banfi, J. Morales, D.L. Armstrong, E.N. Burright, H.T. Orr, J.D. Sweatt, H.Y. Zoghbi, M.M. Matzuk, Mice lacking ataxin-1 display learning deficits and decreased hippocampal paired-pulse facilitation, J. Neurosci. 18 (1998) 5508–5516.
[13] G. Matsumoto, S. Kim, R.I. Morimoto, Huntingtin and mutant SOD1 form aggregate structures with distinct molecular properties in human cells, J. Biol. Chem. 281 (2006) 4477–4485.
[14] J. Nasir, S.B. Floresco, J.R. O'Kusky, V.M. Diewert, J.M. Richman, J. Zeisler, A. Borowski, J.D. Marth, A.G. Phillips, M.R. Hayden, Targeted disruption of the Huntington's disease gene results in embryonic lethality and behavioral and morphological changes in heterozygotes, Cell 81 (1995) 811–823.
[15] S. Zeitlin, J.P. Liu, D.L. Chapman, V.E. Papaioannou, A. Efstratiadis, Increased apoptosis and early embryonic lethality in mice nullizygous for the Huntington's disease gene homologue, Nat. Genet. 11 (1995) 155–163.
[16] E.N. Burright, H.B. Clark, A. Servadio, T. Matilla, R.M. Feddersen, W.S. Yunis, L.A. Duvick, H.Y. Zoghbi, H.T. Orr, SCA1 transgenic mice: a model for neurodegeneration caused by an expanded CAG trinucleotide repeat, Cell 82 (1995) 937–948.
[17] S. Banfi, A. Servadio, M. Chung, F. Capozzoli, L.A. Duvick, R. Elde, H.Y. Zoghbi, H.T. Orr, Cloning and developmental expression analysis of the murine homolog of the spinocerebellar ataxia type 1 gene (Sca1), Hum. Mol. Genet. 5 (1996) 33–40.
[18] A. Servadio, B. Koshy, D. Armstrong, B. Antalffy, H.T. Orr, H.Y. Zoghbi, Expression analysis of the ataxin-1 protein in tissues from normal and spinocerebellar ataxia type 1 individuals, Nat. Genet. 10 (1995) 94–98.
[19] S.L. Hands, A. Wyttenbach, Neurotoxic protein oligomerisation associated with polyglutamine diseases, Acta Neuropathol. 120 (2010) 419–437.
[20] E.S. Emamian, M.D. Kaytor, L.A. Duvick, T. Zu, S.K. Tousey, H.Y. Zoghbi, H.B. Clark, H.T. Orr, Serine 776 of ataxin-1 is critical for polyglutamine-induced disease in SCA1 transgenic mice, Neuron 38 (2003) 375–387.
[21] R.K. Graham, Y. Deng, E.J. Slow, B. Haigh, N. Bissada, G. Lu, J. Pearson, J. Shehadeh, L. Bertram, Z. Murphy, S.C. Warby, C.N. Doty, S. Roy, C.L. Wellington, B.R. Leavitt, L.A. Raymond, D.W. Nicholson, M.R. Hayden, Cleavage at the caspase-6 site is required for neuronal dysfunction and degeneration due to mutant huntingtin, Cell 125 (2006) 1179–1191.
[22] X. Gu, E.R. Greiner, R. Mishra, R. Kodali, A. Osmand, S. Finkbeiner, J.S. Steffan, L.M. Thompson, R. Wetzel, X.W. Yang, Serines 13 and 16 are critical determinants of full-length human mutant huntingtin induced disease pathogenesis in HD mice, Neuron 64 (2009) 828–840.
[23] M. Katsuno, H. Adachi, A. Kume, M. Li, Y. Nakagomi, H. Niwa, C. Sang, Y. Kobayashi, M. Doyu, G. Sobue, Testosterone reduction prevents phenotypic expression in a transgenic mouse model of spinal and bulbar muscular atrophy, Neuron 35 (2002) 843–854.
[24] H. Tsuda, H. Jafar-Nejad, A.J. Patel, Y. Sun, H.K. Chen, M.F. Rose, K.J. Venken, J. Botas, H.T. Orr, H.J. Bellen, H.Y. Zoghbi, The AXH domain of Ataxin-1 mediates neurodegeneration through its interaction with Gfi-1/Senseless proteins, Cell 122 (2005) 633–644.
[25] J. Lim, J. Crespo-Barreto, P. Jafar-Nejad, A.B. Bowman, R. Richman, D.E. Hill, H.T. Orr, H.Y. Zoghbi, Opposing effects of polyglutamine expansion on native protein complexes contribute to SCA1, Nature 452 (2008) 713–718.
[26] L. Duvick, J. Barnes, B. Ebner, S. Agrawal, M. Andresen, J. Lim, G.J. Giesler, H.Y. Zoghbi, H.T. Orr, SCA1-like disease in mice expressing wild-type ataxin-1 with a serine to aspartic acid replacement at residue 776, Neuron 67 (2010) 929–935.
[27] Y. Hirakura, R. Azimov, R. Azimova, B.L. Kagan, Polyglutamine-induced ion channels: a possible mechanism for the neurotoxicity of Huntington and other CAG repeat diseases, J. Neurosci. Res. 60 (2000) 490–494.
[28] H. Monoi, S. Futaki, S. Kugimiya, H. Minakata, K. Yoshihara, Poly-L-glutamine forms cation channels: relevance to the pathogenesis of the polyglutamine diseases, Biophys. J. 78 (2000) 2892–2899.
[29] K.B. Kegel, V. Schewkunow, E. Sapp, N. Masso, E.E. Wanker, M. DiFiglia, W.H. Goldmann, Polyglutamine expansion in huntingtin increases its insertion into lipid bilayers, Biochem. Biophys. Res. Commun. 387 (2009) 472–475.
[30] E. Fedorova, D. Zink, Nuclear genome organization: common themes and individual patterns, Curr. Opin. Genet. Dev. 19 (2009) 166–171.
[31] K. Mekhail, D. Moazed, The nuclear envelope in genome organization, expression and stability, Nat. Rev. Mol. Cell Biol. 11 (2010) 317–328.
[32] M. Mora, L. Cartegni, C. Di Blasi, R. Barresi, S. Bione, M. Raffaele di Barletta, L. Morandi, L. Merlini, V. Nigro, L. Politano, M.A. Donati, F. Cornelio, F. Cobianchi, D. Toniolo, X-linked Emery–Dreifuss muscular dystrophy can be diagnosed from skin biopsy or blood sample, Ann. Neurol. 42 (1997) 249–253.
[33] B. Ravikumar, R. Duden, D.C. Rubinsztein, Aggregate-prone proteins with polyglutamine and polyalanine expansions are degraded by autophagy, Hum. Mol. Genet. 11 (2002) 1107–1117.
[34] J.L. Hutter, J. Bechhoefer, Calibration of atomic-force microscope tips, Rev. Sci. Instrum. 64 (1993) 1868–1873.
[35] C. Canale, M. Jacono, A. Diaspro, S. Dante, Force spectroscopy as a tool to investigate the properties of supported lipid membranes, Microsc. Res. Tech. 73 (2010) 965–972.
[36] M.I. Gurr, J.B. Finean, J.N. Hawthorne, The phospholipids of liver-cell fractions. I. The phospholipid composition of the liver-cell nucleus, Biochim. Biophys. Acta 70 (1963) 406–416.
[37] J.S. Gilchrist, G.N. Pierce, Identification and purification of a calcium-binding protein in hepatic nuclear membranes, J. Biol. Chem. 268 (1993) 4291–4299.
[38] P.J. Skinner, B.T. Koshy, C.J. Cummings, I.A. Klement, K. Helin, A. Servadio, H.Y. Zoghbi, H.T. Orr, Ataxin-1 with an expanded glutamine tract alters nuclear matrix-associated structures, Nature 389 (1997) 971–974.
[39] L. Cartegni, M.R. di Barletta, R. Barresi, S. Squarzoni, P. Sabatelli, N. Maraldi, M. Mora, C. Di Blasi, F. Cornelio, L. Merlini, A. Villa, F. Cobianchi, D. Toniolo, Heart-specific localization of emerin: new insights into Emery–Dreifuss muscular dystrophy, Hum. Mol. Genet. 6 (1997) 2257–2264.
[40] E.N. Burright, H.B. Clark, A. Servadio, A. Matilla, R.M. Feddersen, W.S. Yunis, L.A. Duvick, H.Y. Zoghbi, H.T. Orr, SCA1 transgenic mice: a model for neurodegeneration caused by an expanded CAG trinucleotide repeat, Cell 82 (1995) 937–948.
[41] M. Jayaraman, R. Kodali, R. Wetzel, The impact of ataxin-1-like histidine insertions on polyglutamine aggregation, Protein Eng. Des. Sel. 22 (2009) 469–478.
[42] B.L. Kagan, Amyloidosis and protein folding, Science 307 (2005) 42–43.
[43] H. Jang, J. Zheng, R. Nussinov, Models of beta-amyloid ion channels in the membrane suggest that channel formation in the bilayer is a dynamic process, Biophys. J. 93 (2007) 1938–1949.
[44] B.L. Kagan, R. Azimov, R. Azimova, Amyloid peptide channels, J. Membr. Biol. 202 (2004) 1–10.
[45] J.I. Kourie, A.L. Culverson, P.V. Farrelly, C.L. Henry, K.N. Laohachai, Heterogeneous amyloid-formed ion channels as a common cytotoxic mechanism: implications for therapeutic strategies against amyloidosis, Cell Biochem. Biophys. 36 (2002) 191–207.
[46] A. Quist, I. Doudevski, H. Lin, R. Azimova, D. Ng, B. Frangione, B. Kagan, J. Ghiso, R. Lal, Amyloid ion channels: a common structural link for protein-misfolding disease, Proc. Natl. Acad. Sci. U. S. A. 102 (2005) 10427–10432.